

Čerenkov nonlinear diffraction in random nonlinear photonic crystal of strontium tetraborate

A. M. Vyunishev, A. S. Aleksandrovsky, A. I. Zaitsev, and V. V. Slabko

Citation: *Appl. Phys. Lett.* **101**, 211114 (2012); doi: 10.1063/1.4767385

View online: <http://dx.doi.org/10.1063/1.4767385>

View Table of Contents: <http://apl.aip.org/resource/1/APPLAB/v101/i21>

Published by the [American Institute of Physics](#).

Related Articles

Observation of quantum Talbot effect from a domain-engineered nonlinear photonic crystal
Appl. Phys. Lett. **101**, 211115 (2012)

Self-induced spin-polarized carrier source in active photonic device with artificial optical chirality
Appl. Phys. Lett. **101**, 181106 (2012)

Nanocrystalline diamond photonics platform with high quality factor photonic crystal cavities
Appl. Phys. Lett. **101**, 171115 (2012)

Quasiresonant excitation of InP/InGaP quantum dots using second harmonic generated in a photonic crystal cavity
Appl. Phys. Lett. **101**, 161116 (2012)

Enhancement of photocurrent in ultrathin active-layer photodetecting devices with photonic crystals
Appl. Phys. Lett. **101**, 161103 (2012)

Additional information on *Appl. Phys. Lett.*

Journal Homepage: <http://apl.aip.org/>

Journal Information: http://apl.aip.org/about/about_the_journal

Top downloads: http://apl.aip.org/features/most_downloaded

Information for Authors: <http://apl.aip.org/authors>

ADVERTISEMENT

AIP | Applied Physics
Letters

EXPLORE WHAT'S NEW IN APL

SUBMIT YOUR PAPER NOW!

SURFACES AND INTERFACES
Focusing on physical, chemical, biological, structural, optical, magnetic and electrical properties of surfaces and interfaces, and more...

ENERGY CONVERSION AND STORAGE
Focusing on all aspects of static and dynamic energy conversion, energy storage, photovoltaics, solar fuels, batteries, capacitors, thermoelectrics, and more...

Čerenkov nonlinear diffraction in random nonlinear photonic crystal of strontium tetraborate

A. M. Vyunishev,^{1,2} A. S. Aleksandrovsky,^{1,2} A. I. Zaitsev,^{1,2} and V. V. Slabko²

¹*L.V. Kirensky Institute of Physics, 660036 Krasnoyarsk, Russia*

²*Siberian Federal University, 660079 Krasnoyarsk, Russia*

(Received 28 September 2012; accepted 30 October 2012; published online 21 November 2012)

Čerenkov-type second harmonic generation of femtosecond pulses in random one-dimensional nonlinear photonic crystal of strontium tetraborate is investigated experimentally and theoretically. Sidebands in angular-spectral dependence of generated second harmonic were detected and found to be in perfect agreement with calculations. Spectral maximum of generated radiation experiences deviation from Čerenkov relation due to influence of nonlinear photonic crystal structure. Pulse duration and local spectrum of Čerenkov second harmonic are measured and found to be in fair agreement with each other. © 2012 American Institute of Physics.

[<http://dx.doi.org/10.1063/1.4767385>]

Nonlinear photonic crystals (NPCs),¹ which are the media with the spatial modulation of the second order nonlinear susceptibility, have great potential to convert and to manipulate radiations in photonics.^{2,3} Among different schemes of phase matching attainable in NPCs Čerenkov nonlinear diffraction (CND) is under extensive study in recent years (see, e.g., Refs. 4–14). CND is observed when fundamental wave induced nonlinear polarization travels faster in a normally dispersive medium than harmonic wave. It can be observed in single crystals¹⁴ as well as in periodic and random NPCs. Random NPCs are somewhat more favorable as compared to periodic ones when broadband and widely tunable fundamental radiation is to be converted using CND process. The feature of CND is strong dependence of the internal diffraction angle upon fundamental radiation wavelength,^{4,8,9,12} which is defined by Čerenkov relation $\cos\theta_2 = 2|\mathbf{k}_1|/|\mathbf{k}_2|$, where \mathbf{k}_1 and \mathbf{k}_2 are the wavevectors of fundamental frequency (FF) and second harmonic (SH) wave. This phenomenon can be treated as Čerenkov rainbow¹⁴ or nonlinear superprism (NSP) effect^{4,8,9} since angular dispersion typical for CND can be several orders higher than that in common dispersive devices.^{8,9} Recently, cascaded third harmonic generation (THG) was observed in the CND scheme in two-dimensional (2D) NPC of lithium niobate¹⁵ as well as in random strontium barium niobate (SBN) crystal,¹⁶ and appropriate spectral dependence of the CND deflection angle was measured for this process.¹⁶ In case of broadband pumping an angular chirp (AC) must be present within generated radiation beam. The presence of angular chirp was revealed experimentally by Deng *et al.*^{17,18} using periodically poled lithium niobate (PPLN). The theory of nonlinear diffraction was developed for nanosecond pulses^{19–21} and for more general case of femtosecond ones,²² but the latter still was not used for the study of spectral features of femtosecond pulses generated via CND. One may expect that while in single crystals the spectrum of SH generated under CND conditions will be governed by Čerenkov relation, in NPCs it will be determined by combined action of Čerenkov relation and influence of NPC structure. Random 1D NPC of strontium tetraborate (SBO) is attractive for these studies. Up to now, random NPCs of

SBO are found to be useful for widely tunable broadband frequency conversion^{11,23} and for ultrashort pulse measurements.^{24,25} Frequency converters based on NPC SBO demonstrate super-noncritical phase matching behavior both on angular and wavelength tuning.²⁶ SBO is transparent down to 125 nm, the shortest fundamental absorption edge wavelength among all nonlinear crystals, and, therefore, it is promising for VUV applications. Domains found in SBO can be as thin as 100 nm, the value that still cannot be obtained in ferroelectrics via poling technique. Antiparallel domains formed in ferroelectrics via electric field switching at the temperature well below the temperature of ferroelectric transition typically have rather thick domain walls due to formation of charged layers, being the source of residual electric field component normal to domain walls. This effect can lead to the enhancement of $\chi^{(2)}$ in the vicinity of domain wall. That enhancement was observed in Ref. 17. In this case the function describing $\chi^{(2)}$ dependence on the coordinate becomes more complex. Oppositely, for as-grown domains formed at the temperature close to the melting point, like in case of SBO, one can expect that compensation of residual field will be more efficient. Therefore, domain walls in SBO are expected to be much thinner than in case of electric field switching in ferroelectrics and are not expected to have increased nonlinearity. Particularly, no effect of finite domain wall thickness was found in the analysis of tuning curve of deep ultraviolet radiation generated in NPC SBO.²³

In experiments, we used sample of NPC SBO with the dimensions $6 \times 3.5 \times 3.8$ mm³ along the crystallographic axes a , b , and c , respectively. Sample contained sequence of naturally grown domains with the normal to the domain walls in the direction of a axis. Femtosecond Ti:sapphire oscillator Spectra-Physics Tsunami (repetition rate 82 MHz, average power up to 820 mW, pulse duration 80 fs) was used as the source of fundamental radiation. Spatial profiles of fundamental and SH beams were monitored by Newport LBP-1 beam profiler. Spectral properties of radiations were measured by Solar MSDD1000, Ocean Optics USB4000, HR4000, and Maya 2000Pro spectrometers. Wavelength scale of spectrometers was precisely calibrated prior to measurements. Fundamental radiation was directed along b

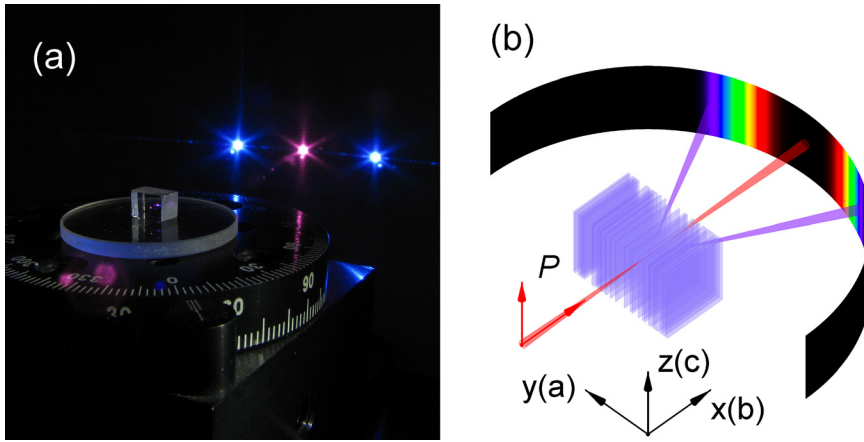


FIG. 1. (a) CND pattern on the screen placed 5 cm after the NPC. The central spot is the fundamental beam passed through the NPC. Two peripheral bright spots are the SH beams projections onto the screen. (b) Experimental geometry. Pseudocolor spectrum on the screen is an illustration of the angular chirp.

axis of SBO. Polarization of fundamental wave coincided with the polar crystallographic axis c to utilize maximum nonlinear coefficient d_{ccc} of SBO. Fig. 1(a) presents the CND pattern observed on the screen placed behind the NPC under study. Two well-shaped SH beams were generated when focused fundamental radiation passed through the NPC.

For theoretical description of CND phenomenon we used classical Akhmanov spectral amplitude approach recently modified for the case of nonlinear diffraction.²² We assumed that the fundamental pulse propagates along x axis (b axis of SBO) as shown in Fig. 1(b). Then, under assumption of nondepletion of the fundamental wave and slowly varying amplitude approximation for the SH wave, the SH field amplitude is governed by

$$\begin{aligned} (\partial/\partial x + \partial/u_2 \partial t + i/2k_2 \nabla_{\perp}^2) A_2(t, x, y) \\ = -ig(\mathbf{r})\beta_2 A_1^2 F^2(\mathbf{r}) F_1^2(t, x) e^{i\Delta k x}, \end{aligned} \quad (1)$$

where $\Delta k = k_2 - 2k_1$ is phase mismatch between SH and fundamental wave, $\nabla_{\perp}^2 = (\partial^2/\partial y^2 + \partial^2/\partial z^2)$ is the transverse Laplacian, A_1 is a maximum field amplitude at the fundamental frequency, $F(\mathbf{r}) = \exp(-r^2/a^2)$ and $F_1(t, x) = \exp(-(t - x/u_1)^2/\tau^2)$ are transverse and longitudinal spatial and temporal profiles of the fundamental pulse field, respectively, 2τ and a are the pulse width and beam radius at 1/e-field strength point, $u_{1,2}$ are the fundamental and SH pulse group velocities, $\beta_2 = 2\pi k_2 \chi^{(2)}/n_2^2$ is nonlinear coupling coefficient, and $g(\mathbf{r})$ is the function responsible for $\chi^{(2)}$ modulation. The second and third terms in the left-hand part of Eq. (1) describe the dispersion and the CND effects. Definition of the function $g(\mathbf{r})$ for typical highly randomized NPC of SBO is complicated; however, if we do not tune the central frequency of the laser, we can approximately consider random NPC as a superposition of several superimposed periodic lattices and choose the periodic structure that gives the main contribution to the CND at given central frequency of the laser. Thickness of domain walls in $g(\mathbf{r})$ function is supposed to be negligibly small, as must be expected for as-grown NPC structure.

By using Fourier transformation, the solution of Eq. (1) can be expressed through its Fourier spectrum as a spectral amplitude $A(\Omega, K, x)$. Thus, expression for the spectral density of the second harmonic $S(\Omega, K, x) = |A(\Omega, K, x)|^2$ is²²

$$\begin{aligned} S(\Omega, K, x) = (|\alpha x|)^2 \exp(-\Omega^2 \tau^2/4) \\ \times \text{sinc}\left(x(\Delta k + \nu\Omega - K^2/2k_2)/2\right)^2 R(K_y), \end{aligned} \quad (2)$$

where $\alpha = \tau a^2 \Gamma(\pi/2)^{3/2}$, $\Gamma = -i\beta_2 I_1$, $\beta_2 = 2\pi k_2 \chi^{(2)}/n_2^2$, and $R(K_y) = (\sum_m g_m \exp(-a^2(mq + K_y)^2/8))^2$, Ω is frequency detuning from the central frequency of SH wave, $\nu = (1/u_2 - 1/u_1)$ is group velocity mismatch, and K_y is reciprocal superlattice vector (RSV).

The spectral dependence for the internal CND angle can be obtained using simple formula

$$\theta_2 = \arccos(n_1/n_2), \quad (3)$$

where n_1 and n_2 are the refractive indices of the FF and SH wave,²⁷ respectively.

Fig. 2 shows experimental and calculated dependences of the external CND angle in the wide spectral range. Experimental data are in agreement with calculated curve using Eq. (3). The CND angle demonstrates strong dependence on the fundamental wavelength and runs up to 90° at the fundamental wavelength 300 nm. For SBO crystal this dependence is shifted to the shorter wavelength range in comparison with the same dependences for lithium niobate and SBN crystals, for which the CND angle runs up to 90° at 760 and 825 nm, respectively. The calculated external angular chirp for SBO

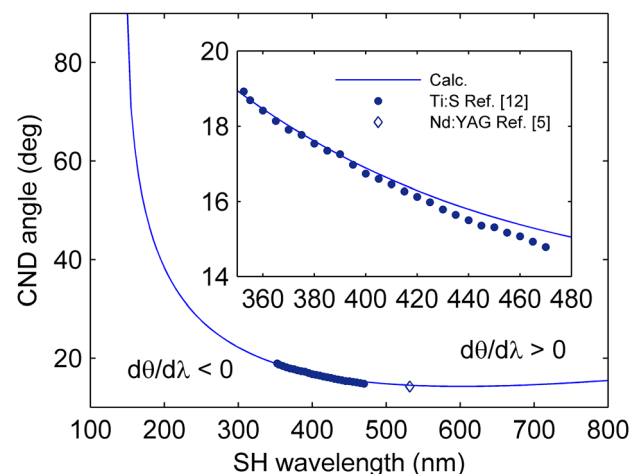


FIG. 2. Spectral dependence of the external CND angle. Solid line is the calculated curve, and points are experimental data from Refs. 5 and 12.

is close to 0.327° per 10 nm at the SH wavelength of 400 nm, which is comparable with angular dispersion of the common prism. At the same time, this feature is expected to be up to several degrees per 10 nm at shorter wavelengths that is higher than angular dispersion of the equilateral prism of the same material in the same spectral region. It is interesting to mention that the angular chirp should change the sign at the fundamental wavelength 1200 nm.

When unfocused fundamental radiation (beam radius 0.45 mm) was directed onto the SBO sample, it produced CND SH radiation with the pattern consisting of several individual beams (Fig. 3(a)). These SH beams are generated by separate parts of random domain structure within fundamental beam section. Therefore, random NPC structure contains several regions with enhanced CND efficiency. The aggregate SH power of all separate beams was measured as a function of coordinate of fundamental beam position in direction normal to domain walls (Fig. 3(c), right Y-axis). When fundamental radiation is focused to $20\ \mu\text{m}$ beam waist radius, then, as a rule, single beam is observed in CND pattern as shown at Fig. 3(b). The SH beam section has elliptic cross-section with a major axis coinciding with the crystallographic axis c . The major beam axis size is determined by fundamental beam divergence, while minor beam axis size is defined by phase matching conditions, i.e., angular width of the Čerenkov noncollinear phase matching. Ellipticity was measured to be about 2. Intensity distribution in SH cross section fits Gaussian function along both axes of elliptic beam spot. The angular divergence of the generated SH beam in the horizontal plane is close to 2 mrad. Scanning the focused beam along a crystallographic axis results in SH power dependence with numerous narrow peaks as shown in Fig. 3(c) (left Y-axis). Maximum average SH power in one

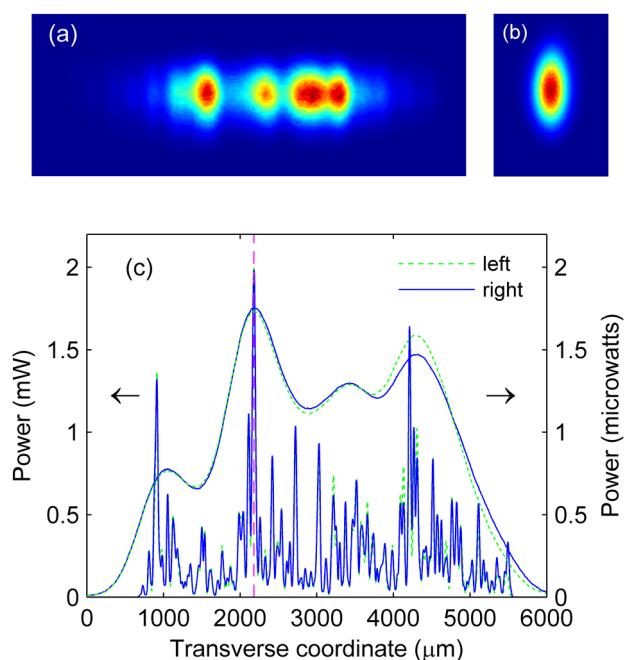


FIG. 3. SH beam profiles with unfocused (a) and focused (b) laser beam. Dependences of averaged SH power on fundamental beam position inside NPC structure (c). Dashed vertical line corresponds to the waist position, where experiments were done (enhanced online) [URL: <http://dx.doi.org/10.1063/1.4767385.1>].

beam was close to 2 mW that corresponds to conversion efficiency of 0.5% in two beams. This is nearly four times smaller than efficiency obtained in Ref. 28 where tighter focusing was used. Subsequent experiments were done when averaged SH power was tuned to maximum with the help of scanning NPC along a axis (dashed line in Fig. 3(c)). The width of SH spectrum was maximum in this case, too.

To measure the SH spectrum distribution across the beam section, an adjustable width slit was used. The SH radiation was focused in the vertical plane with 10-cm focal length cylindrical lens onto the slit. Radiation passing through the slit was completely collected by micro objective into the entrance of optical fiber linked to the spectrometer (MSDD1000, Solar TII or HR4000, Ocean Optics). No noticeable spectral distortions due to diffraction at the slit are expected, as verified by calculations using Fresnel-Kirchhoff integral in Raleigh-Sommerfeld form. The SH spectrum was accumulated during the scanning of the slit position at the pitch of $50\ \mu\text{m}$ in horizontal transverse direction. The slit width was chosen to be $40\ \mu\text{m}$ that is equivalent to the angular interval $0.07\ \text{mrad}$, and measured spectra were averaged within this angular interval. The SH spectra as function of angular position of the slit are plotted in Fig. 4(a). We can see that spectral components are nonuniformly distributed across the beam section, while overall angular and spectral overlaps are smooth. The shorter wavelength components propagate at larger angles according to the CND model.

Corresponding theoretical dependence obtained using Eq. (2) and transformed to wavelength/angle coordinates is presented in Fig. 4(b). These results are found to be very sensitive to input data. Following data were used in the calculation: central wavelength of fundamental radiation 800 nm,

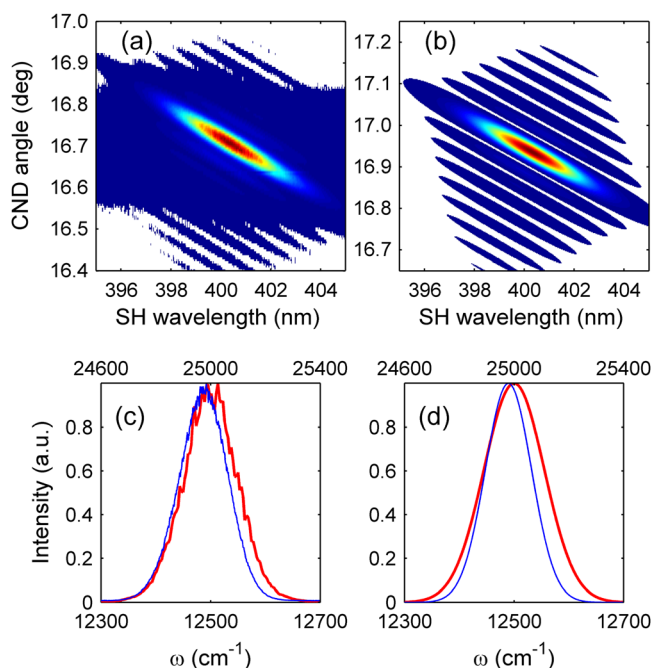


FIG. 4. Measured (a) (FWHM = 3.2 nm; angular width 0.126°) and calculated (b) (FWHM = 3.2 nm; angular width 0.107°) angular dependences of the CND spectral components within SH beam. Background was excluded to reveal the sidebands. Measured (c) and calculated (d) spectra of SH (thin line) and FF (thick line) radiation. Upper scale corresponds to the SH spectrum.

fundamental pulse duration 80 fs, confocal parameter 8.7 mm, fundamental beam waist $40\ \mu\text{m}$ (FWHM), interaction length $3500\ \mu\text{m}$ (equal to the thickness of the sample). Instead of real random structure, periodic structure was used with the RSV $K_y = 4.563\ \mu\text{m}^{-1}$, exactly corresponding to the first order of CND at 800 nm. In spite of the latter simplification, excellent agreement between the shape of measured and calculated spectral intensity plots is evident. Important feature of both experimental and calculated dependences is the existence of “sidebands,” or secondary maxima that look like lower-intensity replicas below and above the main maximum. Calculations show that these sidebands are due to Čerenkov relation but not to NPC structure. While shapes of measured and calculated plots fit well, there is 1.5% difference between measured (16.70° at 800 nm) and calculated CND angles (16.95°). Measured angular chirp was 0.355° per 10 nm, in good agreement with calculated one. Similar scanning of the slit along vertical transverse direction (normal to the RSV plane) showed no angular changes in SH spectra. Another important feature that was found in the experiment is the misfit between maxima of the fundamental and SH spectra (Fig. 4(c)). Maximum of SH spectrum is shifted down by $20\ \text{cm}^{-1}$ ($0.3\ \text{nm}$) with respect to doubled central frequency of the fundamental. This effect cannot be explained by Čerenkov relation and must be ascribed to the influence of NPC structure. This conclusion can be verified by the calculations, the influence of NPC being implemented in the $R(K_y)$ factor in formula (2). Expected shape of SH spectrum calculated for periodic NPC with the period exactly satisfying Čerenkov relation and to the condition of maximum NPC enhancement at 800 nm is presented in Fig. 4(d), in comparison with the squared fundamental spectrum. Therefore, periodic structures designed using Čerenkov relation must give the same spectral misfit. However, this misfit can be compensated by changing the central wavelength of fundamental that can be tuned to produce coinciding fundamental and SH maxima. Alternatively, proper correction can be done on the stage of NPC structure designing so that corrected period of structure enabled maxima coincidence for given central wavelength. For example, $20\ \text{cm}^{-1}$ frequency misfit must be compensated by increasing the RSV value of the structure under construction by 0.35%, for the material with refractive index coinciding with SBO. Good coincidence between SH spectrum calculations and experiment mentioned above supports the use of thin-wall $g(\mathbf{r})$ function in the calculations.

Angular chirp in the CND SH generation process is the origin of complex spatio-temporal coupling in the propagating SH pulse that includes pulse front tilt, and hence, its constituents, temporal down chirp and spatial chirp. This coupling can be detected by measuring local spectrum width within SH beam. For this purpose we measured full width of generated SH spectrum as function of slit width to show that FWHM of the spectrum at the SH beam center converges to the minimum of 1.1 nm as depicted in Fig. 5. Solid line represents calculations using formula (2). This spectral limitation gives calculated transform-limited SH pulse duration close to 214 fs. In the same time, whole spectrum width (3.2 nm) allows to maintain SH pulse duration as short as 75 fs. To measure second harmonic pulse duration we carried out cross-correlation measurements by mixing fundamental

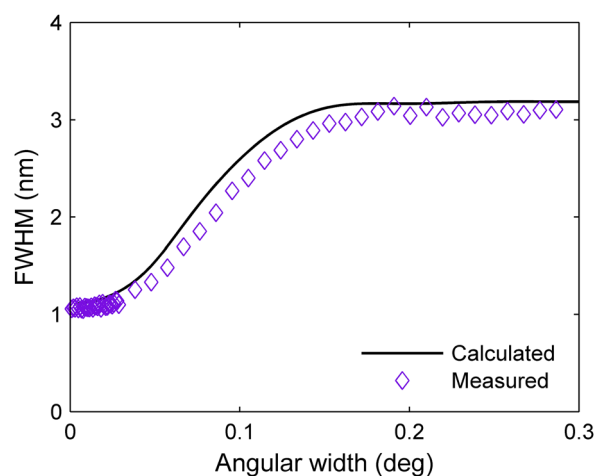


FIG. 5. FWHM of generated and calculated SH spectrum on slit width.

and SH radiation in 0.1 mm-thick BBO crystal. For this measurement, it is very important to ensure perfect spatial overlapping of both beams. We found that cross-correlation signal at the wavelength of the third harmonic (central wavelength 267 nm) is extremely sensitive to the adjustment of optical scheme. The widest cross-correlation function is fitted well by Gaussian function with FWHM of $\tau_{CC} = 214.5$ fs. Therefore, using formula $\tau_2 = \sqrt{\tau_{CC}^2 - \tau_1^2}$ we evaluated the FWHM of unknown second harmonic pulses as 199 fs. Corresponding time-bandwidth product was 1.2. The shortest SH pulse duration that could be retrieved in the course of our measurements was 170 fs. Both these values are smaller than expected from local spectrum width. This discrepancy can be understood in the sense of conclusion obtained in Ref. 29. It was established that if a part of the measured beam is involved in the autocorrelation measurement then not global but local duration is measured, and this value is shorter than the global pulse duration of spatio-temporally coupled pulse. Therefore, it is likely that exact duration of SH pulse is determined by local spectrum and is close to 214 fs.

In conclusion, we have studied the Čerenkov nonlinear diffraction of the femtosecond pulses in random 1D NPC of strontium tetraborate. Sidebands in the angular-spectral dependence of CND power are detected. Deviation of SH spectrum maximum off Čerenkov relation is observed experimentally and was explained by the influence of NPC structure. Akhmanov spectral amplitude approach is proved to be valid for modeling the spectra of SH generated under CND conditions in NPCs. These results must be taken into account while designing both periodic and random NPCs. Local spectral width within the CND SH beam and CND SH pulse duration were measured and found to be in fair agreement. Theoretical approach used may be extended to the calculations of 2D NPCs. Čerenkov nonlinear superprism effect may be used for dispersion management in nonlinear photonics.

The work was supported by RFBR through the Grant No. 12-02-31167, by the Ministry of Education and Science of Russian Federation (Contract No. 14.B37.21.0730 and Grant No. 2.1.1/3455), by RAS Projects 24.29 and 24.31, by PSB RAS Projects 2.5.2 and 3.9.5, by SB RAS Projects 43 and 101, and by SFU Grant F12.

- ¹V. Berger, *Phys. Rev. Lett.* **81**, 4136 (1998).
- ²A. Arie and N. Voloch, *Laser Photon. Rev.* **4**, 355 (2010).
- ³T. Ellenbogen, N. Voloch-Bloch, A. Ganany-Padowicz, and A. Arie, *Nat. Photonics* **3**, 395 (2009).
- ⁴R. Fischer, S. M. Saitiel, D. N. Neshev, W. Krolikowski, and Yu. S. Kivshar, *Appl. Phys. Lett.* **89**, 191105 (2006).
- ⁵A. S. Aleksandrovsky, A. M. Vyunishev, A. I. Zaitsev, A. V. Zamkov, and V. G. Arkhipkin, *J. Opt. A, Pure Appl. Opt.* **9**, S334 (2007).
- ⁶K. A. Kuznetsov, G. Kh. Kitaeva, A. V. Shevlyuga, L. I. Ivleva, and T. R. Volk, *JETP Lett.* **87**, 98 (2008).
- ⁷Y. Zhang, Z. D. Gao, Z. Qi, S. N. Zhu, and N. B. Ming, *Phys. Rev. Lett.* **100**, 163904 (2008).
- ⁸P. Molina, M. Ramírez, and L. Bausá, *Adv. Funct. Mater.* **18**, 709 (2008).
- ⁹P. Molina, S. Álvarez-García, M. O. Ramírez, J. García-Solé, L. E. Bausá, H. Zhang, W. Gao, J. Wang, and M. Jiang, *Appl. Phys. Lett.* **94**, 071111 (2009).
- ¹⁰S. M. Saitiel, Y. Sheng, N. Voloch-Bloch, D. N. Neshev, W. Krolikowski, A. Arie, K. Koynov, and Y. S. Kivshar, *IEEE J. Quantum Electron.* **45**, 1465 (2009).
- ¹¹A. S. Aleksandrovsky, A. M. Vyunishev, V. V. Slabko, A. I. Zaitsev, and A. V. Zamkov, *Opt. Commun.* **282**, 2263 (2009).
- ¹²A. S. Aleksandrovsky, A. M. Vyunishev, A. I. Zaitsev, A. A. Ikonnikov, G. I. Pospelov, V. E. Rovskii, and V. V. Slabko, *Opt. Spectrosc.* **111**, 150 (2011).
- ¹³H. Ren, X. Deng, Y. Zheng, N. An, and X. Chen, *Phys. Rev. Lett.* **108**, 223901 (2012).
- ¹⁴A. A. Kaminskii, H. Nishioka, K. Ueda, W. Odajima, M. Tateno, K. Sasaki, and A. V. Butashin, *Quantum Electron.* **26**, 381 (1996).
- ¹⁵Y. Sheng, W. Wang, R. Shiloh, V. Roppo, Y. Kong, A. Arie, and W. Krolikowski, *Appl. Phys. Lett.* **98**, 241114 (2011).
- ¹⁶M. Ayoub, P. Roedig, J. Imbrock, and C. Denz, *Appl. Phys. Lett.* **99**, 241109 (2011).
- ¹⁷X. Deng, H. Ren, H. Lao, and X. Chen, *Appl. Phys. B* **100**, 755 (2010).
- ¹⁸X. Deng, H. Ren, H. Lao, and X. Chen, *J. Opt. Soc. Am. B* **27**, 1475 (2010).
- ¹⁹Y. Sheng, V. Roppo, Q. Kong, K. Kalinowski, Q. Wang, C. Cojocar, J. Trull, and W. Krolikowski, *Opt. Lett.* **36**, 2593 (2011).
- ²⁰Y. Sheng, Q. Kong, V. Roppo, K. Kalinowski, Q. Wang, C. Cojocar, and W. Krolikowski, *J. Opt. Soc. Am. B* **29**, 312 (2012).
- ²¹K. Kalinowski, P. Roedig, Y. Sheng, M. Ayoub, J. Imbrock, C. Denz, and W. Krolikowski, *Opt. Lett.* **37**, 1832 (2012).
- ²²I. V. Shutov, I. A. Ozheredov, A. V. Shumitski, and A. S. Chirkin, *Opt. Spectrosc.* **105**, 79 (2008).
- ²³A. S. Aleksandrovsky, A. M. Vyunishev, A. I. Zaitsev, and V. V. Slabko, *Phys. Rev. A* **82**, 055806 (2010).
- ²⁴A. S. Aleksandrovsky, A. M. Vyunishev, A. I. Zaitsev, A. A. Ikonnikov, and G. I. Pospelov, *Appl. Phys. Lett.* **98**, 061104 (2011).
- ²⁵A. S. Aleksandrovsky, A. M. Vyunishev, A. I. Zaitsev, G. I. Pospelov, and V. V. Slabko, *Appl. Phys. Lett.* **99**, 211105 (2011).
- ²⁶A. S. Aleksandrovsky, A. M. Vyunishev, and A. I. Zaitsev, *Crystals* **2**, 1393 (2012).
- ²⁷Yu. S. Oseledchik, A. L. Prosvirnin, A. I. Pisarevskiy, V. V. Starshenko, V. V. Osadchuk, S. P. Belokry, N. V. Svitanko, A. S. Korol, S. A. Krikunov, and A. F. Selevich, *Opt. Mater.* **4**, 669 (1995).
- ²⁸A. M. Vyunyshev, A. S. Aleksandrovskii, A. V. Cherepakhin, V. E. Rovskii, A. I. Zaitsev, and A. V. Zamkov, *Bull. Lebedev Phys. Inst.* **37**, 85 (2010).
- ²⁹S. Akturk, X. Gu, P. Bownan, and R. Trebino, *J. Opt.* **12**, 093001 (2010).